

Supporting Information

Steering N/S coordination number to accelerate catecholase-like catalysis over low-coordinated Cu site

Meng Yuan,^a Nannan Xia,^b Ziheng Huang,^a Chaofeng Huang,^c Xun Hu,^{*a} Fei He^{*a}

^a School of Material Science and Engineering, University of Jinan, Jinan 250024, China

^b State Key Laboratory of Biobased Material and Green Papermaking, Key Laboratory of Pulp & Paper Science and Technology of Shandong Province/Ministry of Education, Qilu University of Technology (Shandong Academy of Sciences), Jinan 250353, China

^c School of Chemistry and Chemical Engineering/State Key Laboratory Incubation Base for Green Processing of Chemical Engineering, Shihezi University, Shihezi 832000, China

(*) E-mail: xun.hu@outlook.com; mse_hef@ujn.edu.cn

Experimental Section

Chemicals. 3-Amino-5-thiol-1,2,4-triazole (ATT, 98%) and 3-thiol-1,2,4-triazole (TT, 97%) was purchased from Macklin. 3,5-di-tert-butylcatechol (3,5-DTBC, 98%) and 3,5-di-tert-butylbenzoquinone, (3,5-DTBO, 98%) were purchased from Energy Chemical (Shanghai, China) and Bidepharm, respectively. CuSO₄ was purchased from DAMAO. Ultrapure water was obtained using a Taiping-M pure water purification system (China). All solvents were of analytical grade and used without further purification.

Preparation of ATT-Cu: 2.0 g 3-amino-5-thiol-1,2,4-triazole (ATT) in 125 mL DMF was added in the CuSO₄ aqueous solution (1.36 g CuSO₄ in 250 mL H₂O). After stirred for 24h at room temperature, the mixture was centrifuged, rinsed with H₂O, ethanol and diethyl ether successively. The resulting product was further dried at 100 °C under vacuum to yield ATT-Cu (0.66 g).

Preparation of TT-Cu: 2.0 g 3-thiol-1,2,4-triazole (TT) in 125 mL H₂O was added in the CuSO₄ aqueous solution (1.58 g CuSO₄ in 250 mL H₂O). After stirred for 24h at room temperature, the mixture was centrifuged, rinsed with H₂O, ethanol and diethyl ether successively. The resulting product and dried at 100 °C under vacuum to yield TT-Cu (0.30 g).

Evaluation of the catalytic kinetics: The intrinsic catalytic activity of nanozyme was quantitatively

evaluated based on the kinetics constants, including K_m (substrate affinity), V_{max} (maximal reaction rate), K_{cat} (catalytic rate constant) and K_{cat}/K_m (catalytic efficiency). These kinetics constants were obtained by non-linear curve fitting of Michaelis–Menten equation, which was given as follow:

$$V = V_{max} \times [S]/(K_m + [S])$$

where V and V_{max} represented the initial and maximal reaction velocities, respectively. $[S]$ was the concentration of substrate. K_{cat} was obtained according to the equation: $K_{cat} = V_{max}/[E]$, where $[E]$ represented the concentration of nanozyme.

10 μ L of nanozyme (1 mg mL⁻¹) and 1.5~25 μ L of 3,5-DTBC (50 mM) were added to 500 μ L of acetonitrile/PBS (pH=8) buffer solution with a volume ratio of 1:5. The characteristic absorption peak at 416 nm attributable to 3,5-DTBQ was monitored over time.

Evaluation of electron transfer capability of nanozyme: 1 mg nanozyme, 20 μ L TCNQ (5 mM) and 980 μ L acetonitrile was mixed at room temperature. After stirred at 80 °C for 20 min, the suspension was centrifuged to obtain the liquid, which was further monitored using UV-vis spectroscopy.

Electrochemical measurement: The electrochemical tests were conducted in a standard three-electrode system using a CHI760E workstation. A rotating disk glassy carbon electrode modified with nanozyme acted as the working electrode. A graphite rod and calomel (saturated KCl) were used as counter and reference electrodes, respectively. The nanozyme dispersed in ethanol (5 mg mL⁻¹) was cast on the pre-polished surface of the rotating glassy carbon electrode (RDE, 5 mm diameter) or the rotating ring-disk electrode (RRDE, 5.61 mm diameter). After dried at RT, 10 μ L of Nafion (0.05 wt %) was further cast on the surface of the electrode. For ORR investigation, the electrolyte was the PBS solution (pH=8.0). When testing the catalytic oxidation of 3,5-DTBC, the PBS (pH=8.0)/CH₃CN solution with a volume ratio of 5:1 was saturated by Ar or O₂ and the concentration of 3,5-DTBC was 1 mM.

According to the linear sweep voltammetry (LSV) of RRDE measurement at 1600 rpm, the H₂O₂ yields and the electron transfer number (n) were calculated based on the following equation^[1]:

$$H_2O_2 (\%) = 200 \times \frac{I_R/N_0}{(I_R/N_0) + I_D}$$

$$n = 4 \times \frac{I_D}{(I_R/N_0) + I_D}$$

where I_D and I_R represented the disk current and ring current, respectively. The N_0 represented the

current collection efficiency of RRDE, which was determined to be 0.29.

Calculation of d-band center: The detail to calculate the d-band center is given as the following equation^[2].

$$d\text{-band center} = \frac{\int N(\varepsilon)\varepsilon d\varepsilon}{\int N(\varepsilon)d\varepsilon}$$

where $N(\varepsilon)$ represents the density of states or the XPS-intensity in our work and ε represents the binding energy.

Evaluation of redox constant (k_s): The k_s value was obtained according to the following Laviron equation^[3]:

$$E_c = E_{1/2} - \frac{RT}{\alpha nF} \times \ln \left(\frac{\alpha nF}{RTk_s} \right) - \frac{RT}{\alpha nF} \times \ln v$$

where E_c and $E_{1/2}$ represented the reduction and the formal potential of 3, 5-DTBC, respectively. R and T corresponded to the universal gas constant and the kelvin temperature, respectively. n was the number of electrons transferred for oxidation of 3, 5-DTBC, which was equal to 2. α and k_s were the transfer coefficient and the kinetic constant of 3, 5-DTBC, respectively. v was the scan rate in the CV measurement.

Characterizations

Nitrogen adsorption/desorption test was performed at 77 K using Quantachrome NOVA 1200e (USA) instrument. Before testing, ATT-Cu and TT-Cu were treated via vacuum degassing for 6h at 120°C. Contact angle was tested on a JC2000D1 instrument (China). X-ray photoelectron spectroscopy (XPS) spectra was conducted on a Thermo Scientific K-Alpha (USA) with $h\nu$ 1486.6 eV. Ultraviolet photoelectron spectroscopy (UPS) was conducted on a Thermo Fisher Scientific ESCALAB XI+ (USA). Electron spin resonance (ESR) was carried out on Bruker EMXnano (Germany). Transmission electron microscopy (TEM) image was collected on a JEM-2100 Plus microscope (JEOL, Japan). Scanning electron microscopy (SEM) images were recorded on a ZEISS Gemini 300 (Germany) scanning electron microscope at an acceleration voltage of 3 kV. Energy dispersive X-ray spectroscopy was obtained on an OXFORD XPLORE30 at an acceleration voltage of 15 kV. UV-vis absorption spectroscopy was measured on a UV-2600i UV-vis spectrophotometer (Japan).

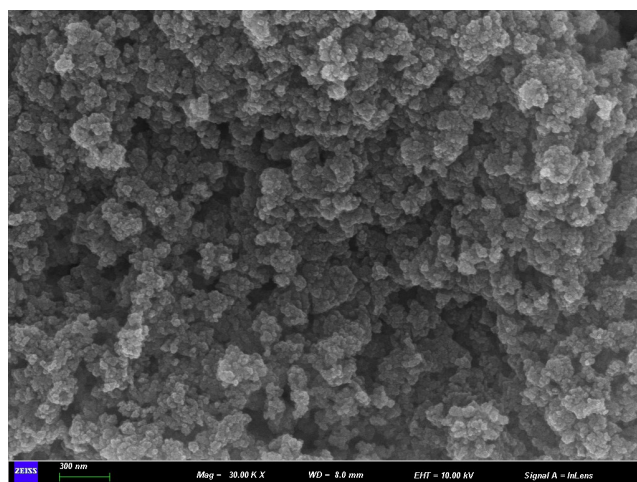


Figure S1 SEM image of TT-Cu.

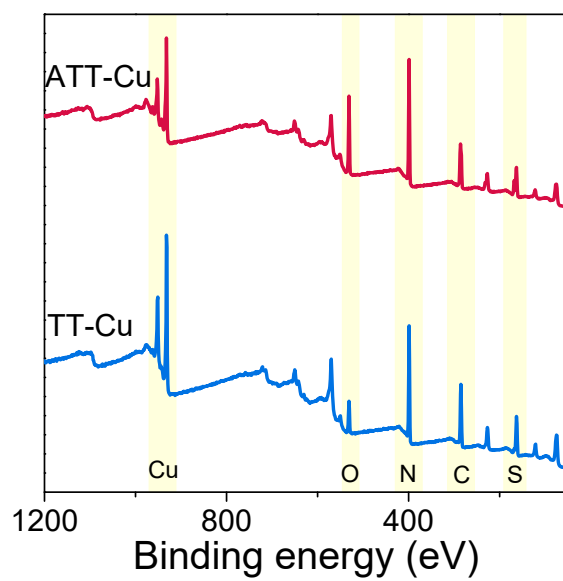


Figure S2 XPS survey spectra of ATT-Cu and TT-Cu.

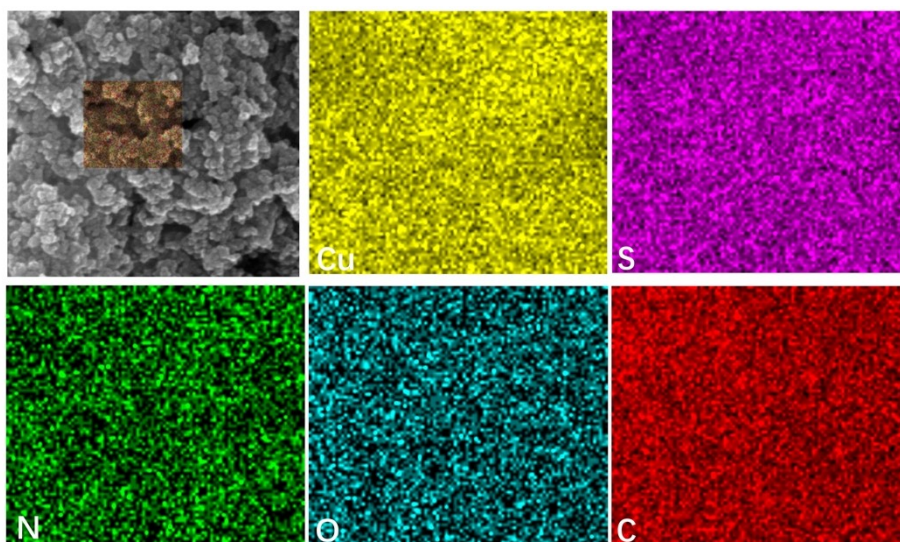


Figure S3 EDS mapping of TT-Cu.

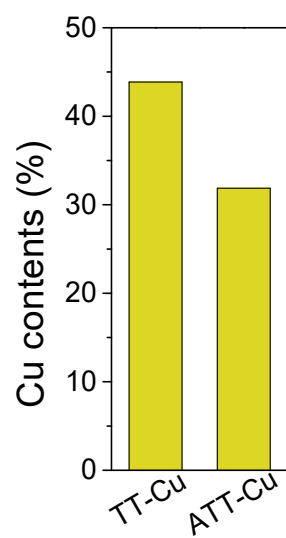


Figure S4 Cu contents (ICP-OES) of ATT-Cu and TT-Cu.

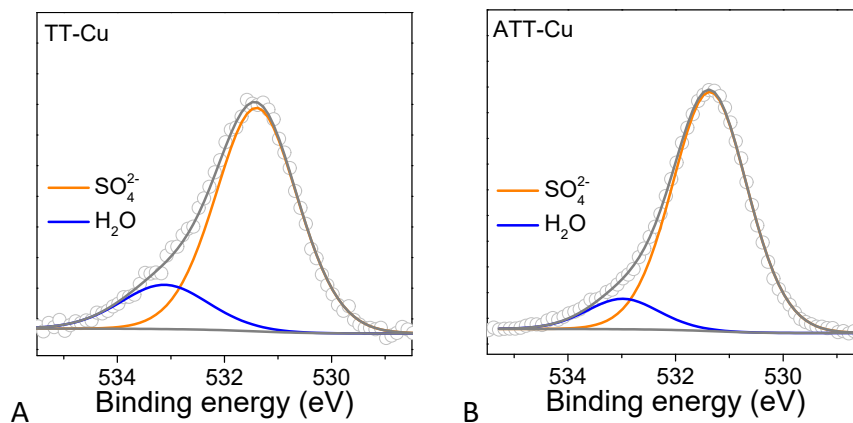


Figure S5 O1s spectra of ATT-Cu and TT-Cu.

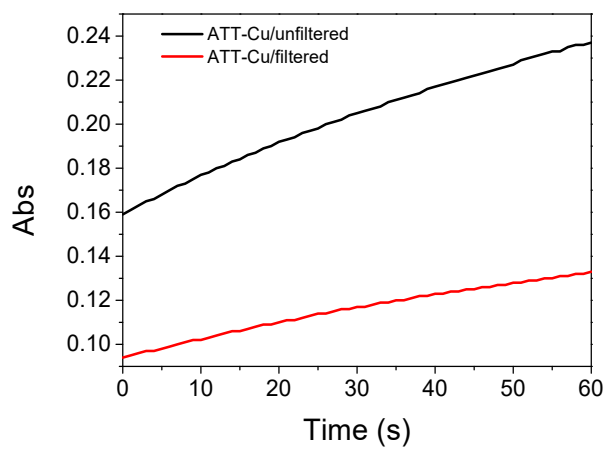


Figure S6 CO-mimicking activities of ATT-Cu before and after filtering with a membrane (pore size: 100nm).

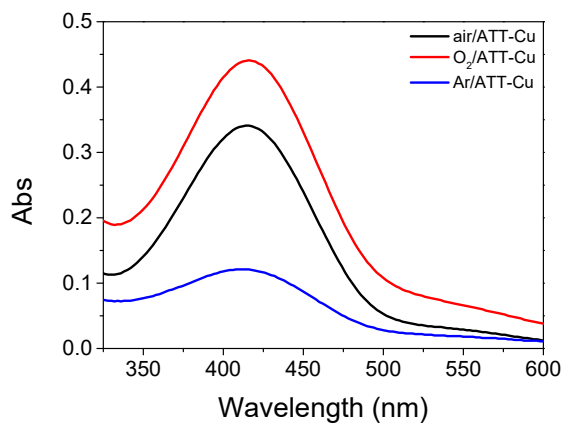


Figure S7 UV-vis spectra of ATT-Cu-catalyzed oxidation of 3,5-DTBC in Ar, air and O₂.

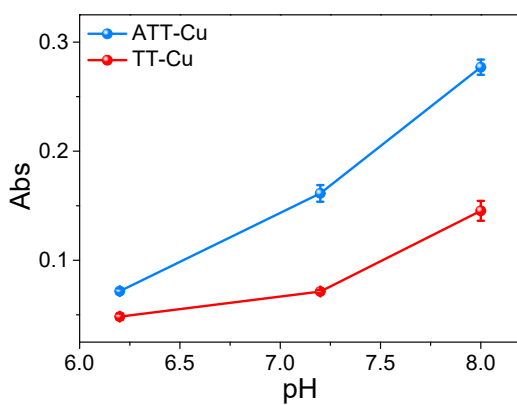


Figure S8 CO-mimicking activities of ATT-Cu under different pH condition.

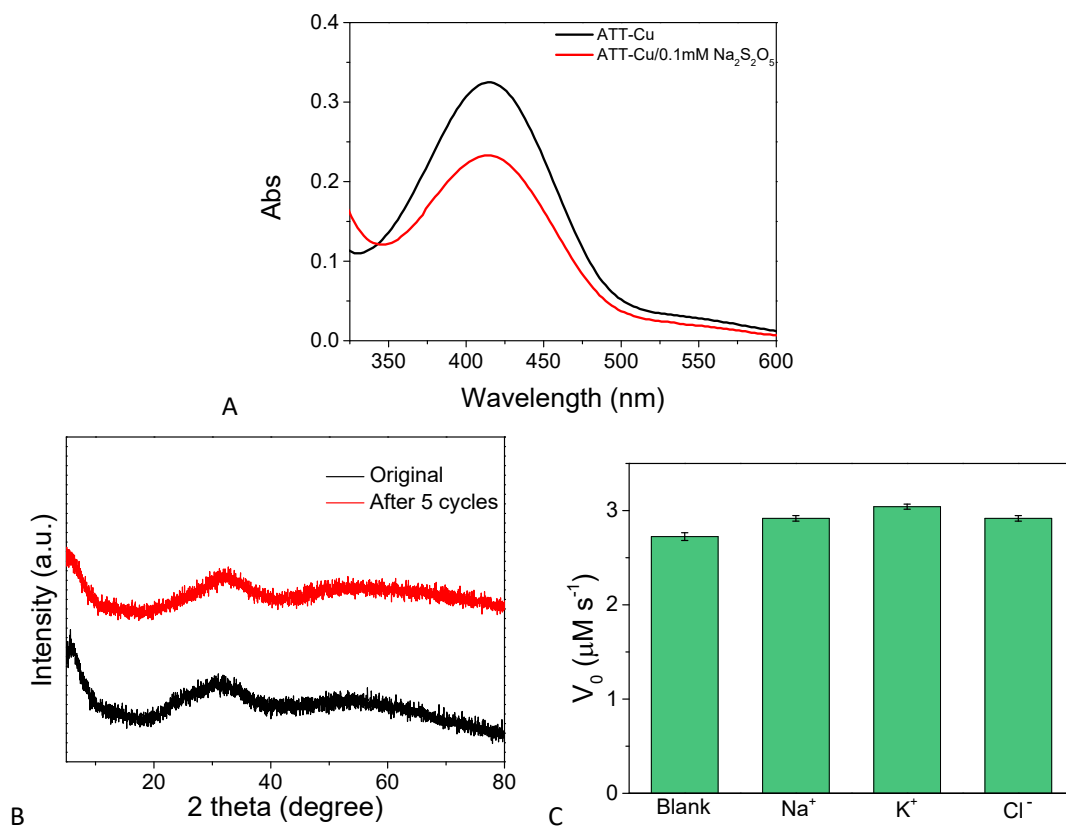


Figure S9 (A) UV-vis spectra of ATT-Cu-catalyzed oxidation of 3,5-DTBC before and after Na₂S₂O₅ inhibiting; (B) XRD patterns of ATT-Cu before and after cycle tests; (C) Anti-interference capabilities of ATT-Cu for K⁺, Na⁺ and Cl⁻ during mimicking CO-like catalysis.

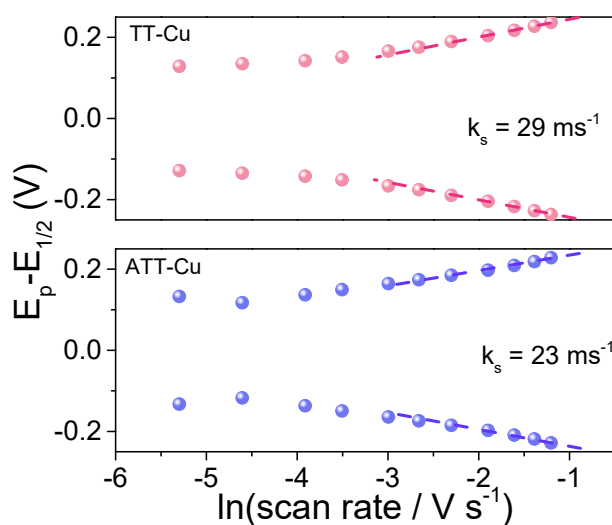


Figure S10 Pots of the redox peak potentials versus the logarithm of scan rates.

Table S1 EXAFS fitting parameters at the Cu *K*-edge for ATT-Cu, TT-Cu and Cu foil.

Sample	Shell	CN^a	$R(\text{\AA})^b$	$\sigma^2(\text{\AA}^2)^c$	$\Delta E_0(\text{eV})^d$	<i>R</i> factor
Cu-foil	Cu-Cu	12*	2.54±0.01	0.0083±0.0005	3.9±0.6	0.0033
TT-Cu	Cu-N	1.2±0.2	1.88±0.01	0.0103±0.0020	-3.1±0.4	0.0047
	Cu-S	2.5±0.4	2.22±0.01			
ATT-Cu	Cu-N	2.0±0.3	1.93±0.01	0.0005±0.0022	2.0±0.6	0.0145
	Cu-S	0.5±0.1	2.29±0.01			

^a*CN*, coordination number; ^b*R*, the distance to the neighboring atom; ^c σ^2 , Debye-Waller factor, the Mean Square Relative Displacement (MSRD); ^d ΔE_0 , inner potential correction; *R* factor indicates the goodness of the fit. S_0^2 was fixed to 0.809, according to the experimental EXAFS fit of Cu foil by fixing *CN* as the known crystallographic value. * This value was fixed during EXAFS fitting, based on the known structure of Cu. Fitting range: $3.0 \leq k (\text{\AA}^{-1}) \leq 12.0$ and $1.0 \leq R (\text{\AA}) \leq 2.8$ (Cu foil); $2.0 \leq k (\text{\AA}^{-1}) \leq 10.5$ and $1.0 \leq R (\text{\AA}) \leq 2.2$ (Cu-TT); $2.0 \leq k (\text{\AA}^{-1}) \leq 10.5$ and $1.0 \leq R (\text{\AA}) \leq 2.2$ (Cu-ATT). A reasonable range of EXAFS fitting parameters: $0.700 < S_0^2 < 1.000$; $CN > 0$; $\sigma^2 > 0 \text{\AA}^2$; $|\Delta E_0| < 15 \text{ eV}$; *R* factor < 0.02.

Table S2 Comparison of CO-mimicking activities between ATT-Cu and other reported artificial enzymes

Species	$K_m(\mu\text{M})$	$K_{\text{cat}} (\text{s}^{-1})$	$K_{\text{cat}}/K_m (\text{mM}^{-1} \text{s}^{-1})$	Ref.
Cu-P1	380	8.23×10^{-6}	3.578×10^{-5}	[4]
Cu-P2	230	1.44×10^{-5}	6.231×10^{-5}	[4]
Cu-P3	800	2.03×10^{-5}	2.538×10^{-5}	[4]
Cu-P4	960	1.93×10^{-5}	2.01×10^{-5}	[4]
Cu-P5	910	2.18×10^{-5}	2.34×10^{-5}	[4]
Cu-GMADPA	220	3.23×10^{-6}	1.468×10^{-5}	[4]
MOF-808-L-His-Cu	2210	0.0069	0.00312	[5]
CeO ₂	1262	6.28×10^{-4}	4.98×10^{-4}	[6]
PtNPs	1818	0.0184	0.0101	[6]
MOF-818	810	0.0384	0.0474	[6]
CA-Cu	2240	0.364	0.1625	[7]
Fmoc-K/GMP/Cu ²⁺	453	1.196	2.4247	[8]
DT-Cu	152	0.114	0.749	[9]
Ce-MOF-818	2589	1.25	0.482	[10]
Zr-MOF-818	2054	0.8	0.391	[10]
Ce-MOF-808	2453	0.24	0.0959	[10]
MOF-808-His-Cu	85.07	0.04679	0.55	[11]
ATT-Cu	499.6	0.03362	0.0673	this work

References

- [1] F. He, L. Mi, Y. Shen, X. Chen, Y. Yang, H. Mei, S. Liu, T. Mori, Y. Zhang, *J. Mater. Chem. A* **2017**, *5*, 17413-17420.
- [2] S. J. Hwang, S. K. Kim, J. G. Lee, S. C. Lee, J. H. Jang, P. Kim, T. H. Lim, Y. E. Sung, S. J. Yoo, *J. Am. Chem. Soc.* **2012**, *134*, 19508-19511.
- [3] P. Ei Phyu Win, J. Yang, S. Ning, X. Huang, G. Fu, Q. Sun, X. H. Xia, J. Wang, *Proc. Natl. Acad. Sci. U. S. A.* **2024**, *121*, e2316553121.

- [4] S. Thanneeru, N. Milazzo, A. Lopes, Z. Wei, A. M. Angeles-Boza, J. He, *J. Am. Chem. Soc.* **2019**, *141*, 4252-4256.
- [5] M. Sha, L. Rao, W. Xu, Y. Qin, R. Su, Y. Wu, Q. Fang, H. Wang, X. Cui, L. Zheng, *Nano Lett.* **2023**, *23*, 701-709.
- [6] M. Li, J. Chen, W. Wu, Y. Fang, S. Dong, *J. Am. Chem. Soc.* **2020**, *142*, 15569-15574.
- [7] J. Wang, R. Huang, W. Qi, R. Su, Z. He, *Chem. Eng. J.* **2022**, *434*, 134677.
- [8] S. Xu, H. Wu, S. Liu, P. Du, H. Wang, H. Yang, W. Xu, S. Chen, L. Song, J. Li, *Nat. Commun.* **2023**, *14*, 4040.
- [9] M. Yuan, K. Han, H. Yang, L. Mi, C. Huang, X. Hu, F. He, *Small* **2024**, e2401756.
- [10] S. Liu, Y. He, W. Zhang, T. Fu, L. Wang, Y. Zhang, Y. Xu, H. Sun, H. Zhao, *Small* **2024**, *20*, e2306522.
- [11] R. V. Morajkar, A. P. Fatrekar, A. A. Vernekar, *Chem. Sci.* **2024**, doi: 10.1039/D4SC02136C.